Synthesis, Crystal Structure, NMR Studies, and Thermal Stability of Mixed Iron−Indium Phosphates with Quasi-One-Dimensional Frameworks

X. Tang, A. Jones, and A. Lachgar*

Department of Chemistry, Wake Forest University, Winston-Salem, North Carolina 27109

B. J. Gross and J. L. Yarger

Department of Chemistry, University of Wyoming, Laramie, Wyoming 82071

Received May 24, 1999

The hydrothermal synthesis, single-crystal structure analysis, spectroscopic studies, and thermal stability of the compounds $Ca_2(In_{1-x}Fe_x)(PO_4)(HPO_4)_2{\cdot}H_2O$ ($0 \le x \le 1$) are reported. The framework of these new phases is based on linear chains (//[101]) formed by (MO_6) octahedra and (PO_4)/(HPO_4) tetrahedra sharing corners. The (HPO_4) groups and water molecules link the chains through hydrogen bonding to form layers stacked perpendicular to the *c* axis. The calcium cations are located between the layers and are coordinated by nine oxide anions. Crystal data: $Ca_2In(PO_4)(HPO_4)_2{\cdot}H_2O$, space group *C*2/*c* (No. 15), $a = 7.573(1)$ Å, $b = 15.838(1)$ Å, $c = 9.3126(7)$ Å, $\beta = 113.55(1)°$; $Ca_2(In_{0.5}Fe_{0.5})(PO_4)(HPO_4)_2{\cdot}H_2O$, *C*2/*c* (No. 15), $a = 7.548(2)$ Å, $b = 15.670(3)$ Å, $c = 9.241(2)$ Å, $\beta = 113.62(3)°$; $Ca_2Fe(PO_4)(HPO_4)_2{\cdot}H_2O$, *C*2/*c* (No. 15), $a = 7.503(2)$ Å, $b = 15.477(2)$ Å, $c = 9.142(1)$ Å, $\beta = 113.60(2)°$. The phases lose two water molecules between 350 and 600 °C to form the series $Ca_2(In_{1-x}Fe_x)(PO_4)(P_2O_7)$ ($0 \le x \le 1$), which are isostructural with $Ca_2V(PO_4)(P_2O_7)$. Solid state magic angle spinning (MAS) ^{31}P NMR of $Ca_2In(PO_4)(HPO_4)_2{\cdot}H_2O$ confirms two phosphorous moieties in roughly a 2:1 ratio. A CP-MAS buildup study yielded polarization transfer rates (T_{IS}^{-1}) of 2128 and 1597 s^{-1} for the HPO_4 (−2.4 ppm) and PO_4 (−0.9 ppm) sites, respectively. A $^1H-^{31}P$ WISE experiment indicates the presence of motional narrowing and hydrogen exchange between the water molecules and hydroxyl protons.

Introduction

Fundamental understanding of materials properties and increasing demands for high-performance materials constitute the main reasons for the exploratory synthesis and characterization of open-framework solids.[1−3] In recent years, a few open-framework ternary indium phosphates have been discovered through solid state high-temperature techniques or mild hydrothermal synthesis methods, mainly in the system $A^+-In^{III}-(PO_4)/(AsO_4)$ (A^+ = alkali cation). Examples include $Li_3In_2P_3O_{12}$ and $Li_{1+x}Ti_{2-x}In_xP_3O_{12}$,[4] $Na_3In(PO_4)_2$,[5,6] $Na_3In_2(AsO_4)_3$,[6,7] $NaCdIn_2(PO_4)_3$,[8] $KIn(OH)PO_4$,[9] $RbIn(OH)PO_4$,[10] $RbIn(HPO_4)_2$,[11] and $Cs[In_2(PO_4)(HPO_4)_2(H_2O)_2]$.[12] The compound $Li_{1+x}Ti_{2-x}In_x(PO_4)_3$ is particularly important due to its high Li^+ ion conductivity.[13,14]

Recent investigations of transition metal (M^{III}) phosphates led to the synthesis of a number of new phases with versatile structural properties. For example, $Ca_2V(PO_4)(HPO_4)_2{\cdot}H_2O$ and $Sr_2M(PO_4)_2(H_2PO_4)$ ($M = V^{III}$ or Fe^{III}) have pseudo layered frameworks built up of chains of corner-sharing MO_6 octahedra and phosphate tetrahedra.[15,16] $CaM_2(PO_4)_2(HPO_4)$ ($M = V^{III}$ or Fe^{III}) has a three-dimensional framework built from dimers of edge-sharing MO_6 octahedra and PO_4/HPO_4 tetrahedra.[17] $SrFe_3(PO_4)_3(HPO_4)$ has a framework containing FeO_5 trigonal bipyramids and dimers of face-sharing FeO_6 octahedra.[18] The three-dimensional framework of $BaV_2(HPO_4)_4{\cdot}H_2O$ generates interconnecting tunnels.[19]

Iron phosphates have a wide range of practical applications. They have potential for applications as cathode materials for

(1) Cao, G.; Hong, H.-G.; Mallouk, T. E. *Acc. Chem. Res.* **1992**, *25* (9), 420−427.
(2) Centi, G.; Trifiro, F.; Ebner, J. R.; Franchetti, V. M. *Chem. Rev.* **1988**, *88* (1), 55−80.
(3) Clearfield, A. *Chem. Rev.* **1988**, *88* (1), 125−148.
(4) (a) Tran Qui, D.; Hamdoune, S. *Acta Crystallogr.* **1987**, *C43*, 397−399. (b) Tran Qui, D.; Hamdoune, S. *Acta Crystallogr.* **1988**, *C44*, 1360−1362.
(5) Lii, K.-H. *Eur. J. Solid State Inorg. Chem.* **1996**, *33* (6), 519−526.
(6) Lii, K.-H.; Ye, J. *J. Solid State Chem.* **1997**, *131* (1), 131−137.
(7) Khorari, S.; Rulmont, A.; Tarte, P. *J. Solid State Chem.* **1997**, *134* (1), 31−37.
(8) Antenucci, D.; Miehe, G.; Tarte, P.; Schmahl, W. W.; Fransolet, A.-M. *Eur. J. Mineral.* **1993**, *5* (2), 207−213.
(9) Hriljac, A. C.; Grey, P.; Cheetham, A. K.; VerNooy, P. D.; Torardi, C. C. *J. Solid State Chem.* **1996**, *123* (2), 243−248.
(10) Lii, K.-H. *J. Chem. Soc., Dalton Trans.* **1996**, No. 6, 815−818.
(11) Tang, X.; Lachgar, A. To be published.
(12) Dhingra, S. S.; Haushalter, R. C. *J. Solid State Chem.* **1994**, *112* (1), 96−99.
(13) (a) Aono, H.; Sugimoto, E.; Sadaoka, Y.; Imanaka, N.; Adachi, G.-Y. *J. Electrochem. Soc.* **1990**, *137* (4), 1023−1027. (b) Aono, H.; Sugimoto, E.; Sadaoka, Y.; Imanaka, N.; Adachi, G.-Y. *Bull. Chem. Soc. Jpn.* **1992**, *65* (8), 2200−2204.
(14) Hamdoune, S.; Tran Qui, D. *Solid State Ionics* **1986**, *18* and *19*, 587−591.
(15) Lii, K.-H.; Wen, N. S.; Su, C. C.; Chueh, B. R. *Inorg. Chem.* **1992**, *31* (3), 439−442.
(16) Lii, K.-H.; Lee, T.-C.; Liu, S.-N.; Wang, S.-L. *J. Chem. Soc., Dalton Trans.* **1993**, No. 7, 1051−1054.
(17) Lii, K.-H. *J. Chem. Soc., Dalton Trans.* **1994**, No. 6, 931−935.
(18) Lii, K.-H.; Dong, T.-Y.; Cheng, C.-Y.; Wang, S.-L. *J. Chem. Soc., Dalton Trans.* **1993**, No. 4, 577−580.
(19) Wang, Z.; Haushalter, R. C.; Thompson, M. E.; Zubieta, J. *Mater. Chem. Phys.* **1993**, *35*, 205−207.

10.1021/ic9905906 CCC: $18.00
Published on Web 12/03/1999

rechargeable lithium batteries,[20] materials for fossil energy conversion and sensors,[21] materials for corrosion inhibition and passivation of metal surfaces,[22] and heterogeneous catalysis.[23] Structural studies of iron phosphates have shown that they can form a variety of complex structural types.[24,25] The similarities between In^{3+} and transition metals in the +3 oxidation state suggest that this structural diversity may also exist in the systems $A^{2+}-In^{III}-(PO_4)$ (A^{2+} = alkaline earth cations). Our earlier investigation of this system led to the discovery of $CaIn_2(PO_4)_2(HPO_4)$, whose framework contains In_2O_{10} dimers.[26] Here, we report the hydrothermal synthesis and characterization of the solid solution $Ca_2(In_{1-x}Fe_x)(PO_4)(HPO_4)_2\cdot H_2O$ ($0 \le x \le 1$) whose framework is based on linear chains made up of edge-sharing octahedra and tetrahedra. The chains interact with each other through hydrogen bonding to form layers. Solid state nuclear magnetic resonance (NMR) spectroscopy was used to characterize the phosphorus local environments, the proximity of protons to the phosphate chains, and relative proton mobility. Investigation of their thermal stability using a combination of TGA/DTA and X-ray powder diffraction shows that these compounds can be used as precursors to preparing new mixed-metal phosphates−pyrophosphates.

Experimental Section

Synthesis. $Ca_2In(PO_4)(HPO_4)_2\cdot H_2O$. CaO (0.2244 g) (Alfa, reagent, 95%), 2 mL of 0.5 M $InCl_3$ solution (prepared from $InCl_3$, Aldrich, 98%), 2 mL of 1 M tetramethylammonium hydroxide (TMAOH) solution (prepared from $(CH_3)_4NOH\cdot 5H_2O$, Aldrich, 97%), and 8 mL of 2 M H_3PO_4 solution (prepared from H_3PO_4, Fisher, 85% aqueous solution) were mixed in a 23 mL Teflon-lined stainless steel autoclave. The resulting gel had a molar ratio of $CaO:InCl_3:TMAOH:H_3PO_4$ = 4:1:4:16. The reaction was carried out in a tubular furnace at 190 °C for 3 days and then furnace cooled to room temperature. The product was filtered, washed with water and acetone, and dried at room temperature. It consisted of colorless monoclinic columnlike crystals in 63% yield based on indium.

$Ca_2Fe(PO_4)(HPO_4)_2\cdot H_2O$. $Fe(NO_3)_3$ instead of $InCl_3$ was used for the preparation of $Ca_2Fe(PO_4)(HPO_4)_2\cdot H_2O$. The other chemicals, reaction conditions, and product handling were the same as those used for the preparation of $Ca_2In(PO_4)(HPO_4)_2\cdot H_2O$. The molar ratio of the starting materials was $CaO:Fe(NO_3)_3:TMAOH:H_3PO_4$ = 4:1:4:16. The product was obtained in 76% yield based on Fe. It crystallized as pale-yellow monoclinic needlelike crystals.

$Ca_2(In_{0.5}Fe_{0.5})(PO_4)(HPO4)_2\cdot H_2O$. The compound was prepared using the same method as described above. The molar ratio of the starting materials was $CaO:Fe(NO_3)_3:InCl_3:TMAOH:H_3PO_4$ = 8:1:1:4:32. The product consisted of colorless blocklike crystals. The yield was 63% based on indium or iron.

Elemental Analysis. Energy-dispersive X-ray analyses (EDAX) of the crystalline products were obtained using a Philips 515 scanning electron microscope equipped with a microprobe. The analyses confirmed the presence of Ca, In (or Fe), and P. No chlorine was found.

The phase $Ca_2(In_{0.5}Fe_{0.5})(PO_4)(HPO_4)_2\cdot H_2O$ was analyzed for Fe and In using using a Perkin-Elmer Optima 3100-XL ICP-OES at three Fe wavelengths (238.204, 239.562, and 259.939 nm) and three In wavelengths (230.606, 325.609, and 303.936 nm). The sample (0.0192 g) was dissolved in 25.0 mL of 6 M HCl, and the solution was diluted with distilled, deionized water to a volume of 1000.0 mL. The dilute solution was analyzed at each of the six wavelengths. Calibration curves were calculated for each of the wavelengths using three standards: one blank, one containing 1.00 ppm Fe and In, and one containing 10.0 ppm Fe and In. Results of these analyses are submitted as Supporting Information.

Infrared Absorption Spectroscopy. The IR absorption spectra were recorded in the range between 3600 and 400 cm^{-1} using KBr pellets on a Mattson Instrument 4020 Galaxy FT-IR with Enhanced FIRST software.

Thermal Analysis. The thermal stability of $Ca_2(In_{1-x}Fe_x)(PO_4)(HPO_4)_2\cdot H_2O$ (x = 0, 0.5, 1) was investigated using a Netzsch STA 409 TGA/DTA apparatus. Samples were heated under nitrogen flow (22 mL/min) to 900 °C at 5 °C/min and then cooled to room temperature at 20 °C/min. $Ca_2In(PO_4)(HPO_4)_2\cdot H_2O$ loses a total of 7.2% in two not-well-resolved endothermic steps. The study indicates a one-step endothermic weight loss of 7.6% and 7.9% for the compounds $Ca_2(In_{0.5}Fe_{0.5})(PO_4)(HPO_4)_2\cdot H_2O$ and $Ca_2Fe(PO_4)(HPO_4)_2\cdot H_2O$, respectively. The thermal decomposition products were analyzed using a Philipps X-ray powder diffractometer (Cu Kα radiation).

Crystal Structure Determination. $Ca_2In(PO_4)(HPO_4)_2\cdot H_2O$. A colorless monoclinic columnlike single crystal of $Ca_2In(PO_4)(HPO_4)_2\cdot H_2O$ was mounted in a thin-walled glass capillary for diffraction studies.

Table 1. Crystal Data and Structure Refinement Data for $Ca_2(In_{1-x}Fe_x)(PO_4)(HPO_4)_2\cdot H_2O$ (x = 0, 0.5, 1)

	$x = 0$	$x = 0.5$	$x = 1$
formula	$Ca_2In(PO_4)(HPO_4)_2\cdot H_2O$	$Ca_2In_{0.5}Fe_{0.5}(PO_4)(HPO_4)_2\cdot H_2O$	$Ca_2Fe(PO_4)(HPO_4)_2\cdot H_2O$
a (Å)	7.573(1)	7.548(2)	7.503(2)
b (Å)	15.838(1)	15.670(3)	15.477(2)
c (Å)	9.3126(7)	9.241(2)	9.142(1)
β (deg)	113.55(1)	113.62(3)	113.60(2)
V (Å^3)	1024.0(2)	1001.5(4)	972.8(3)
Z	4	4	4
fw	499.92	470.44	440.95
space group	$C2/c$ (No. 15)	$C2/c$ (No. 15)	$C2/c$ (No. 15)
T (K)	298(1)	298(1)	298(1)
λ (Å)	0.71073	0.71073	0.71073
ρ_{calcd} (g cm^{-3})	3.243	3.120	3.011
μ (g cm^{-3})	38.5	35.1	31.8
R1[a]	0.031	0.030	0.027
wR2[b,c]	0.073	0.074	0.069

[a] $R_1 = \sum||F_o| - |F_c||/\sum|F_o|$. [b] $wR2 = [\sum[w(F_o^2 - F_c^2)^2]/\sum[(wF_o^2)^2]]^{1/2}$. [c] $w^{-1} = \sigma^2(F_o^2) + (aP)^2 + bP$ where $P = (\mathrm{Max}(F_o^2,0) + 2F_c^2)/3$, a = 0.028 and b = 0.00 for $Ca_2In(PO_4)(HPO_4)_2\cdot H_2O$, a = 0.038 and b = 2.17 for $Ca_2(In_{0.5}Fe_{0.5})(PO_4)(HPO_4)_2\cdot H_2O$, and a = 0.034 and b = 0.71 for $Ca_2Fe(PO_4)(HPO_4)_2\cdot H_2O$.

Table 2. Atomic Coordinates, Equivalent Isotropic Displacement Parameters (Å^2), and Bond Valence Sums for $Ca_2In(PO_4)(Hpo_4)_2\cdot H_2O$

	x	y	z	U(eq)	$\sum s$[a]
In	0.25	0.25	0.5	0.00816(9)	3.23
Ca	0.27075(9)	0.49214(4)	0.56442(8)	0.0142(1)	2.00
P(1)	0	0.40189(7)	0.25	0.0076(2)	5.06
P(2)	0.1746(1)	0.14741(5)	0.15174(9)	0.0094(2)	5.01
O(1)	0.0330(4)	0.4559(2)	0.1289(3)	0.0184(5)	2.12
O(2)	0.1842(4)	0.3495(2)	0.3374(3)	0.0179(5)	1.86
O(3)	0.0827(4)	0.0606(2)	0.1200(3)	0.0208(5)	1.93
O(4)	0.2651(4)	0.1610(2)	0.3278(3)	0.0214(5)	1.93
O(5)	0.0445(4)	0.2194(2)	0.0622(3)	0.0167(5)	1.84
O(6)	0.3335(4)	0.1378(2)	0.0829(3)	0.0196(5)	1.26
O(7)	0.5	0.5976(3)	0.75	0.0207(8)	0.43
H(1)	0.36(−)	0.184(−)	0.06(−)	0.03(−)	
H(21)	0.60(1)	0.626(6)	0.77(2)	0.03(3)	
H(22)	0.54(2)	0.622(6)	0.70(1)	0.02(3)	

[a] Bond valence sums were calculated without hydrogen.

(20) Masquelier, C.; Padhi, A. K.; Nanjundaswamy, K. S.; Goodenough, J. B. *J. Solid State Chem.* **1998**, *135*, 228−234.

(21) Lazoryak, B. I. In *Fundamental Study of New Materials and Processes in the Substances*; Moscow University Press: Moscow, 1994; p 54.

(22) (a) Meisel, W.; Mohs, E.; Guttmann, H. J.; Gütlish, P. *Corros. Sci.* **1983**, *23* (5), 465−471. (b) Attali, S.; Vigouroux, B.; Lenzi, M.; Persia, J. *J. Catal.* **1980**, *63* (2), 496−500.

(23) Moffat, J. B. *Catal. Rev. Sci. Eng.* **1978**, *18* (2), 199−258.

(24) (a) Moore, P.; Shen, J. *Nature* **1983**, *306*, 356−358. (b) Moore, P. In *The Second International Congress on Phosphorus Compounds Proceedings*, April 21−25, 1980; p 105.

(25) (a) Lii, K.-H.; Huang, C. *J. Chem. Soc., Dalton Trans.* **1995**, No. 4, 571−574. (b) Gabelica-Robert, M.; Goreaud, M.; Labbe, Ph.; Raveau, B. *J. Solid State Chem.* **1982**, *45* (3), 389−395.

(26) Tang, X.; Lachgar, A. *Z. Anorg. Allg. Chem.* **1996**, *622* (3), 513−517.

Table 3. Selected Bond Distances (Å) and Angles (deg) for $Ca_2In(PO_4)(HPO_4)_2 \cdot H_2O$[a]

InO_6 Octahedron

In	O(2)[a]	O(2)	O(5)[b]	O(5)[c]	O(4)	O(4)[a]
O(2)[a]	2.103(2)	180.00	86.9(1)	93.1(1)	88.8(1)	91.2(1)
O(2)		2.103(2)	93.1(1)	86.9(1)	91.2(1)	88.8(1)
O(5)[b]			2.124(3)	180.00	90.6(1)	89.4(1)
O(5)[c]				2.124(3)	89.4(1)	90.6(1)
O(4)					2.172(3)	180.00
O(4)[a]						2.172(3)

$P(1)O_4$ Tetrahedron

P(1)	O(1)[b]	O(1)	O(2)[b]	O(2)
O(1)[b]	1.513(2)	111.2(2)	108.2(2)	107.1(2)
O(1)		1.513(2)	107.1(2)	108.2(1)
O(2)[b]			1.546(3)	115.0(2)
O(2)				1.546(3)

$P(2)O_4$ Tetrahedron

P(2)	O(3)	O(4)	O(5)	O(6)
O(3)	1.516(3)	108.3(2)	115.3(2)	101.5(2)
O(4)		1.518(3)	113.6(2)	111.3(2)
O(5)			1.520(3)	106.3(2)
O(6)				1.580(3)

Ca−O Bond Lengths

Ca−O(1)[d]	2.268(3)	Ca−O(7)	2.528(3)	Ca−O(4)[a]	2.681(3)
Ca−O(1)[b]	2.356(3)	Ca−O(3)[e]	2.623(3)	Ca−O(3)[a]	2.821(3)
Ca−O(3)[c]	2.360(3)	Ca−O(6)[e]	2.639(3)	Ca−O(2)	2.983(3)

H Bonds

O(6)−H(1)	0.82(−)	H(1)···O(5)	2.18(−)	O(6)···O(5)	2.965(4)
O(7)−H(21)	0.81(6)	H(21)···O(2)	2.30(10)	O(7)···O(2)	2.939(3)
O(7)−H(22)	0.81(6)	H(22)···O(2)	2.25(8)	O(7)···O(2)	2.939(3)

[a] Symmetry codes: (a) $-x + 1/2, -y + 1/2, -z + 1$; (b) $-x, y, -z + 1/2$; (c) $x + 1/2, -y + 1/2, z + 1/2$; (*d*) $x, -y + 1, z + 1/2$; (e) $-x + 1/2, y + 1/2, -z + 1/2$.

The data were collected at room temperature on a Siemens P4 diffractometer with Mo Kα radiation ($\lambda = 0.71073$ Å). The unit cell parameters were determined from centering and least-squares refinements of 45 randomly chosen reflections between 6 and 30° in 2θ: Intensity data were collected on a monoclinic unit cell using an $\omega-2\theta$ scan mode with variable scan rate between 4 and 20°/min. A total of 5653 reflections were collected with a maximum 2θ of 60° for the sphere $\pm h, \pm k, \pm l$. The crystal showed no detectable decay during the data collection as monitored by periodically measuring the intensities of three selected standard reflections. The intensity data were corrected for Lorentz and polarization effects, and an empirical absorption correction based on ψ-scans of 10 reflections ($T_{min} = 0.322$, $T_{max} = 0.517$) was applied. The observed systematic absences were found to be consistent with the space groups *C*2/*c* (No. 15) and *Cc* (No. 9). The structure determination and refinement were carried out in the centrosymmetric space group *C*2/*c* using the Shelxtl-plus program package. Direct methods were used to locate calcium, indium, and phosphorus, and the remaining atoms were located from successive Fourier difference maps. All hydrogen atoms were located from a difference Fourier synthesis. The hydrogen atom H(1) of the HPO_4 unit could not be refined independently and was included in the refinement with the constraint that the O(6)−H(1) distance be 0.82 Å. All atoms except hydrogen were refined anisotropically in the final full-matrix least-squares refinements, R1 = 0.031, wR2 = 0.073. The isotropic thermal parameter of H(1) was fixed at a value 1.3 times the equivalent isotropic thermal parameter of its oxygen, O(6). As for the water molecule, two possible hydrogen positions were located from the difference Fourier map, and each was allowed to vary independently with a fixed occupancy of 0.50. The final difference Fourier map showed no significant residual density (maximum 0.76 e·Å^{-3}), indicating that the structure solution is complete. The main crystallographic data are given in Table 1. Atomic positions, bond distances, and bond angles are given in Tables 2 and 3. Refinement of the structure in the polar space group *Cc* gave higher reliability factors, R1 = 0.037 and wR2 = 0.087.

$Ca_2(In_{0.5}Fe_{0.5})(PO_4)(HPO_4)_2 \cdot H_2O$. The crystal handling, data collection and corrections, and structure determination and refinements were the same as above. The structure solution indicates that Fe and In occupy the same crystallographic site (4*d*). Their anisotropic thermal parameters were restrained to be the same, and their occupancies were refined with the restraint that their sum corresponds to the full occupancy of the metal site. The final refinement gave occupancies of 0.537(2) and 0.463(2) for Fe and In, respectively. The hydrogen atom H(1) of the HPO_4 unit could not be refined independently and was included in the refinement with the constraint that the O(6)−H(1) distance be 0.82 Å. The isotropic thermal parameter of H(1) was allowed to vary independently. The hydrogen of the water molecule, H(2), was located from a difference Fourier map; its position and isotropic thermal parameter were refined independently from those of O(7). The main crystallographic data are listed in Table 1. The details of data collection and refinement and bond distances and angles are submitted in CIF format as Supporting Information.

$Ca_2Fe(PO_4)(HPO_4)_2 \cdot H_2O$. The crystal handling, data collection and reduction, and structure determination and refinements were the same as those used for $Ca_2In(PO_4)(HPO_4)_2 \cdot H_2O$. The hydrogen in this structure were found to behave as in the mixed indium−iron isomorph. The main crystallographic data are given in Table 1. The details of data collection and refinement and bond distances and angles are submitted in CIF format as Supporting Information.

Nuclear Magnetic Resonance Spectroscopy. The $Ca_2In(PO_4)(HPO_4)_2 \cdot H_2O$ sample was loaded into a 4 mm zirconia rotor and studied at ambient temperature on a Chemagnetics Infinity 400 MHz NMR spectrometer in a MAS "Pencil Probe" from the same company ($\nu_o(^{31}P) = 161.990$ MHz, $\nu_o(^1H) = 400.171$ MHz). All spectra were taken while spinning at 15 kHz ± 2 Hz and referenced to 85% H_3PO_4 unless otherwise stated. Static and MAS single-pulse Bloch decay spectra were recorded using standard CYCLOPS phase cycling.[27] $^1H-^{31}P$ CP-MAS[28,29] spectra were recorded at the Hartmann−Hahn matching condition (centerband) using a standard spin-locking[30] approach and were detected under ^1H decoupling. The CP-MAS spectra were recorded with contact times varying from 10 μs to 1.2 ms. A 2D $^{31}P-^1H$ wide-line separation (WISE) experiment using a rotor frequency of 10 kHz

(27) Cavanagh, J.; Fairbrother, W. J.; Palmer, A. G., III; Skelton, N. J. *Protein NMR Spectroscopy Principles and Practice*; Academic Press: New York, 1996.
(28) Pines, A.; Gibby, M. G.; Waugh, J. S. *J. Chem. Phys.* **1973**, *59*, 569.

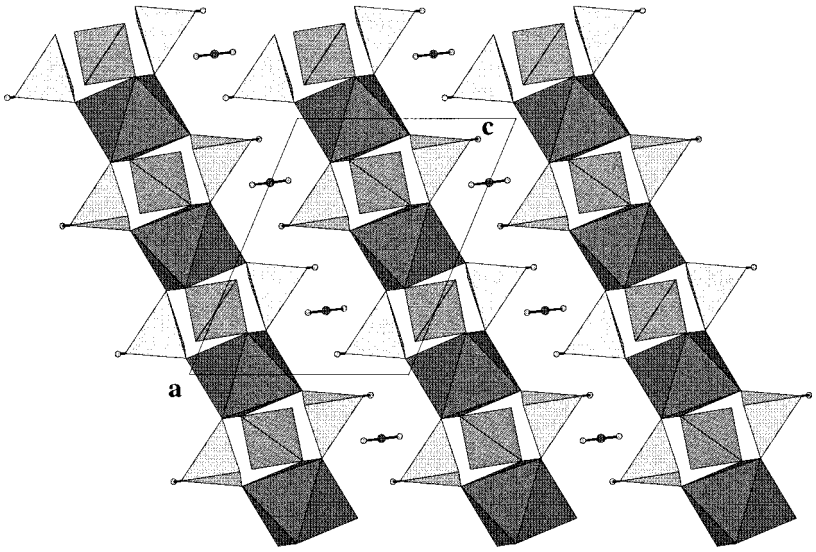

Figure 1. Projection along the *b* axis of one layer formed through hydrogen bonding of the [−O−3T−] chains in $Ca_2In(PO_4)(HPO_4)_2 \cdot H_2O$. The chains are parallel to the [101] direction, and the water molecules are located between adjacent chains.

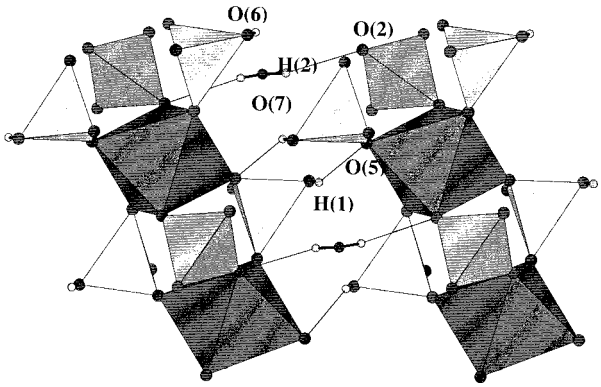

Figure 2. Representation of the hydrogen bonding between neighboring chains. Hydrogen bonding occurs through water molecules and HPO_4 groups.

was conducted using the pulse sequence and phase cycling of K. Schmidt-Rohr et al.[31]

Results and Discussion

Structural Description. The three compounds reported here are isostructural and represent three members of a solid solution between $Ca_2In(PO_4)(HPO_4) \cdot H_2O$ and $Ca_2Fe(PO_4)(HPO_4) \cdot H_2O$. Here a detailed description of the structure of $Ca_2In(PO_4)(HPO_4) \cdot H_2O$ is given. Crystallographic data for the three compounds are reported as a CIF file.

The framework of $Ca_2In(PO_4)(HPO_4)_2 \cdot H_2O$ is built of (InO_6) octahedra and (PO_4)/(HPO_4) tetrahedra that share corners to form infinite linear chains running along the [101] crystallographic direction (Figure 1). Adjacent chains are linked to each other through hydrogen bonding via water molecules and (HPO_4) (Figure 2) to form layers stacked parallel to the *ac* plane. The calcium cations are located within the interlayer spacing.

Indium is located at the inversion center and is coordinated by six oxygen atoms in an almost regular octahedral geometry with In−O bond distances between 2.103(2) and 2.124(2) Å. The (InO_6) octahedron shares all six oxo ligands with two ($P(1)O_4$) and four ($HP(2)O_4$) tetrahedra. The tetrahedra ($P(1)O_4$) share two oxygen ligands O(2) with (InO_6) octahedra (P(1)−O(2): 1.546(2) Å); the two remaining ligands O(1) are unshared (P(1)−O(1): 1.513(2) Å). ($HP(2)O_4$) has one long and three short P−O bonds. The crystal structure analysis and bond valence sum calculations[32] (Table 2) show that O(6) bonds to a hydrogen atom to form the hydroxyl ligand of the ($HP(2)O_4$) group. Water molecules O(7) are located between two neighboring chains and form hydrogen bonds with O(2) (Figure 2). Additional hydrogen bonding is formed between two ($HP(2)O_4$)

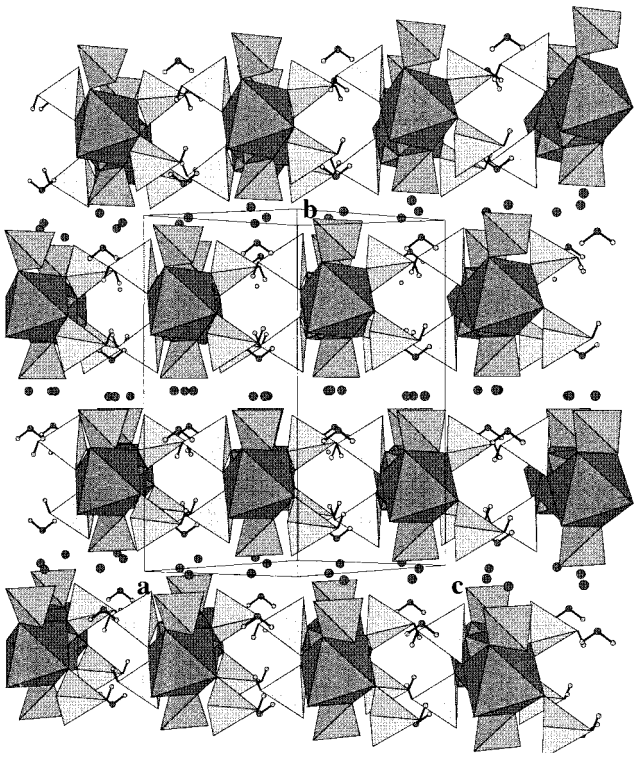

Figure 3. Perspective view of $Ca_2In(PO_4)(HPO_4)_2 \cdot H_2O$ along the [101] direction.

(29) Hartmann, A. R.; Hahn, E. L. *Phys. Rev.* **1962**, *128*, 2024.
(30) Mehring, M. *Principles of High Resolution NMR in Solids*; Springer: Berlin, 1983.
(31) Schmidt-Rohr, K.; Clauss, J.; Spiess, H. W. *Macromolecules* **1992**, *25* (12) 3273−3277.
(32) Altermatt, D.; Brown, I. D. *Acta Crystallogr.* **1985**, *B41*, 240−244.

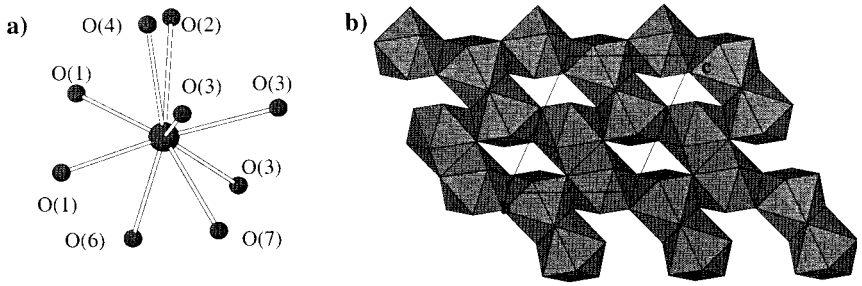

Figure 4. Coordination environment of calcium in $Ca_2In(PO_4)(HPO_4)\cdot H_2O$: (a) nine oxygen atoms surrounding Ca^{2+}; (b) the (CaO_9) polyhedra share edges to generate a 2D network.

Table 4. Hydrogen-Bonding Interactions in $Ca_2(In_{1-x}Fe_x)(PO_4)(HPO_4)_2\cdot H_2O$ ($x = 0$, 0.5, 1)

donor, D	acceptor, A	H···A (Å)	D···A (Å)	D−H···A (deg)	H−D···A (deg)
		$Ca_2In(PO_4)(HPO_4)_2\cdot H_2O$			
O(6)−H(1)	O(5)	2.18	2.965(4)	161	14
O(7)−H(21)	O(2)	2.30(10)	2.939(3)	137(12)	32(9)
O(7)−H(22)	O(2)	2.25(8)	2.939(3)	144(11)	27(9)
		$Ca_2(Fe_{0.5}In_{0.5})(PO_4)(HPO_4)_2\cdot H_2O$			
O(6)−H(1)	O(5)	2.24	2.898(3)	137	32
O(7)−H(2)	O(2)	2.22(4)	2.942(2)	153(4)	20(3)
		$Ca_2Fe(PO_4)(HPO_4)_2\cdot H_2O$			
O(6)−H(1)	O(5)	2.08	2.820(3)	151	21
O(7)−H(2)	O(2)	2.11(5)	2.941(2)	161(5)	14(3)

Table 5. Unit Cell and Bond Length Changes for $Ca_2(In_{1-x}Fe_x)(PO_4)(HPO_4)_2\cdot H_2O$

	$x = 0$	$x = 0.5$	$x = 1$
a (Å)	7.5732	7.548	7.503
b (Å)	15.838	15.670	15.477
c (Å)	9.3126	9.241	9.142
V (Å^3)	1023.9	1001.5	972.8
M−O(2) (Å)	2.103	2.032	1.966
M−O(5) (Å)	2.124	2.072	2.017
M−O(4) (Å)	2.172	2.097	2.020
M−O (Å) (av)	2.133	2.067	2.001
P−O (Å) (av)	1.532	1.534	1.530
Ca−O (Å) (av)	2.584	2.578	2.567

tetrahedra from neighboring chains (O(6)−H(1)···O(5)). Table 4 summarizes the hydrogen-bonding interactions in the three compounds.

The open-framework character of the structure is illustrated in the perspective view shown in Figure 3. The Ca^{2+} cations are located between the layers and coordinate to nine oxygen atoms, forming (CaO_9) polyhedra. Each (CaO_9) polyhedron shares one triangular face and two edges with three neighboring (CaO_9) polyhedra to generate a two-dimensional net of (CaO_9) polyhedra (Figure 4).

The major structural features of $Ca_2(In_{1-x}Fe_x)(PO_4)(HPO_4)_2\cdot H_2O$ ($x = 1$, 0.5) are the same as those described above for $x = 0$. In the case of $x = 0.5$, Fe and In are statistically distributed over the metal site. The unit cell parameters and bond lengths increase as *x* decreases (Table 5), which correlates well with increasing occupancy of the larger metal ion In^{3+}.

Infrared Absorption Spectroscopy. The IR spectra of the three compounds show similar features.

$Ca_2In(PO_4)(HPO_4)_2\cdot H_2O$. 3430 (m), 2300 (m), 1630 (m), 1120 (s), 1065 (s), 1040 (s), 1000 (s), 920 (m), 740 (w), 590 (m), 550 (m).

$Ca_2Fe(PO_4)(HPO_4)_2\cdot H_2O$. 3480 (m), 3070 (m), 2570 (m), 1630 (m), 1130 (s), 1060 (s), 1000 (s), 940 (m), 730 (w), 580 (m), 570 (m), 490 (w).

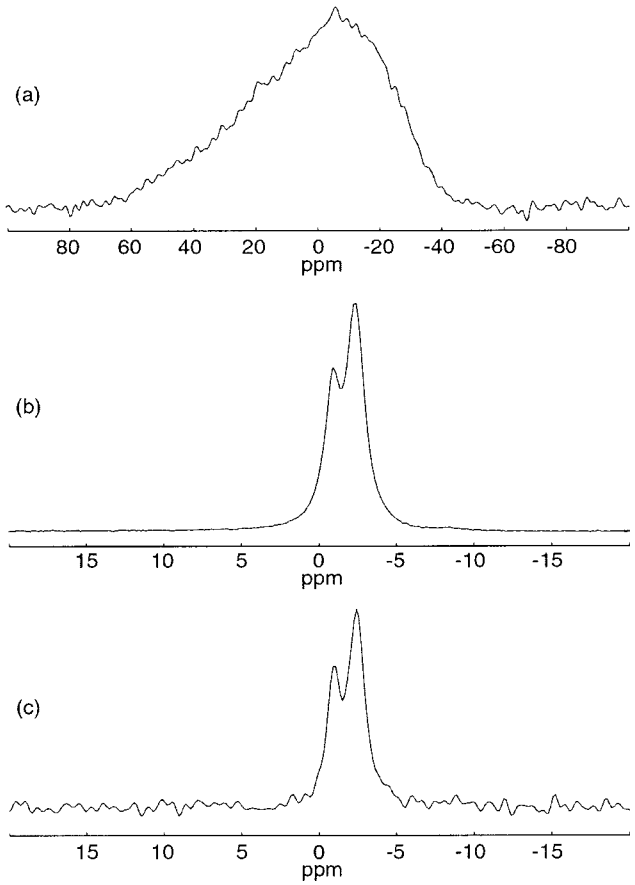

Figure 5. ^{31}P solid state NMR spectra of $Ca_2In(PO_4)(HPO_4)_2\cdot H_2O$ crystalline powder: (a) static single-pulse ^1H-decoupled spectrum; (b) 15 kHz ^1H decoupling; (c) ^1H-decoupled 15 kHz MAS ^{31}P spectrum. All spectra are referenced to 85% H_3PO_4.

$Ca_2(In_{0.5}Fe_{0.5})(PO_4)(HPO_4)_2\cdot H_2O$. 3530 (w), 3200 (m), 2500 (m), 1630 (m), 1130 (s), 1070 (s), 1000 (m), 950 (m), 740 (w), 590 (m), 550 (m).

The absorption bands at 3600−3000 and 2900−2200 cm^{-1} are due to the O−H bond stretch from the water molecule and (HPO_4) groups. The bands at about 1600 cm^{-1} correspond to O−H librations of water molecules. The bands between 1200 and 400 cm^{-1} are due to P−O bond vibrations.

Thermal Stability Studies. The thermal stability of the compounds $Ca_2(In_{1-x}Fe_x)(PO_4)(HPO_4)_2\cdot H_2O$ ($x = 1$, 0.5, 0) was studied using a combination of TGA and DTA techniques. $Ca_2In(PO_4)(HPO_4)_2\cdot H_2O$ shows a two-step weight loss. The first step occurs in the temperature range 350−500 °C and corresponds to a percent weight loss of 4.7%. The second step (2.5%) occurs between 500 and 600 °C. The total weight loss of these two steps (7.2%) agrees with the loss of two water molecules per molecular formula (calculated weight loss = 7.20%). One

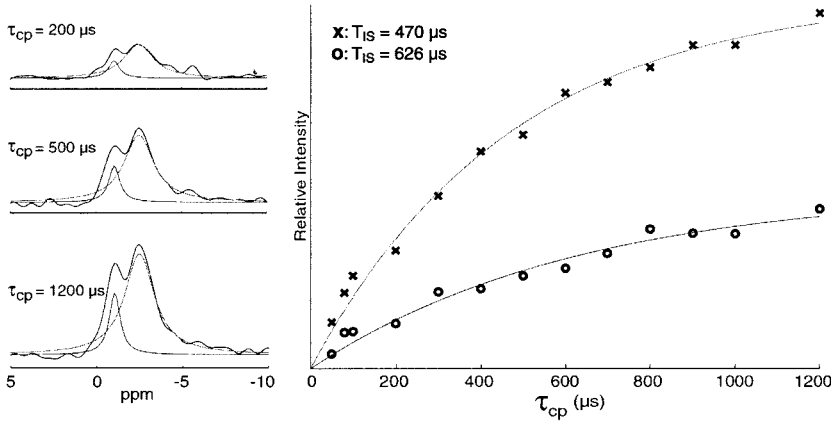

Figure 6. Cross-polarization spectra of $Ca_2In(PO_4)(HPO_4)_2{\cdot}H_2O$. Left side: 1D $^1H-^{31}P$ cross-polarization MAS spectra with varying contact time. The data is fit using a two Lorentzian peak model with fixed chemical shift and peak width values of 125 Hz at −0.9 ppm and 340 Hz at −2.4 ppm for the PO_4 and HPO_4 groups, respectively. Right side: Using the areas extracted from the Lorentzian peak fits and the relative 2:1 peak ratios, the normalized polarization buildup of the two ^{31}P peaks is plotted as a function of contact time. The extracted time constants (T_{IS}) of both components are given.

water molecule comes from the water of crystallization, and the second results from the condensation of two (HPO_4) groups to form a (P_2O_7) group:

$$Ca_2In(PO_4)(HPO_4)_2{\cdot}H_2O \xrightarrow{350-600\ ^\circ C} Ca_2In(PO_4)(P_2O_7) + 2H_2O$$

A third step (% loss ≈ 1%) is exothermic and occurs between 600 and 800 °C. This step could be attributed to the presence of an amorphous impurity which could not be detected by X-ray diffraction.

The product obtained after heating at 900 °C is analyzed by X-ray diffraction. The X-ray powder pattern is indexed on the basis of the calculated powder pattern of the previously reported vanadium pyrophosphate $Ca_2V(PO_4)(P_2O_7)$.[17] Refinement of the unit cell constants based on 45 reflections ($10° < 2\theta < 67°$) leads to a monoclinic unit cell with $a = 6.474(2)$ Å, $b = 6.761(4)$ Å, $c = 19.27(1)$ Å, $\beta = 99.17(4)°$, confirming that the final dehydration product corresponds to the phase $Ca_2In(PO_4)(P_2O_7)$.

The dehydration of $Ca_2Fe(PO_4)(HPO_4)_2{\cdot}H_2O$ occurs in one step at temperatures between 400 and 560 °C. The percent weight loss of 7.9% corresponds to a loss of two water molecules (calculated % weight loss: 8.14%).

$$Ca_2Fe(PO_4)(HPO_4)_2{\cdot}H_2O \xrightarrow{400-560\ ^\circ C} Ca_2Fe(PO_4)(P_2O_7) + 2H_2O$$

As in the case of $Ca_2In(PO_4)(HPO_4)_2{\cdot}H_2O$, a 1% weight loss occurs between 600 and 800 °C. The powder pattern of the dehydration product at 900 °C can be indexed on the basis of the known structure of $Ca_2V(PO_4)(P_2O_7)$. Refinement of cell constants using 39 reflections ($10° < 2\theta < 70°$) yields a monoclinic cell with $a = 6.390(2)$ Å, $b = 6.653(3)$ Å, $c = 19.086(6)$ Å, $\beta = 99.21(4)°$.

$Ca_2(In_{0.5}Fe_{0.5})(PO_4)(HPO_4)_2{\cdot}H_2O$ exhibits thermal behavior similar to that of its iron and indium analogues:

$$Ca_2(Fe_{0.5}In_{0.5})(PO_4)(HPO_4)_2{\cdot}H_2O \xrightarrow{350-550\ ^\circ C} Ca_2(Fe_{0.5}In_{0.5})(PO_4)(P_2O_7) + 2H_2O$$

The dehydration product at 900 °C corresponds to the phase $Ca_2(In_{0.5}Fe_{0.5})(PO_4)(P_2O_7)$. Refinement of the unit cell parameters using 32 reflections with ($10° < 2\theta < 67°$) leads to a monoclinic cell: $a = 6.4480(3)$ Å, $b = 6.727(4)$ Å, $c = 19.46(2)$ Å, $\beta = 99.95(4)°$.

Solid State NMR Studies. Solid state NMR is an excellent probe of the local environment surrounding the nucleus under scrutiny. Figure 5a shows a static ^1H-decoupled ^{31}P NMR spectrum of crystalline $Ca_2In(PO_4)(HPO_4)_2{\cdot}H_2O$ powder. A typical chemical shift anisotropy (CSA) powder pattern is *not* observed, but rather we see a Gaussian broadened CSA pattern. This broadening is due to heteronuclear and homonuclear dipolar interactions. Studying the sample under MAS eliminates the effects of residual homonuclear dipole coupling and largely eliminates the effects of residual heteronuclear dipole coupling, making it possible to clearly resolve the two distinctive ^{31}P environments as displayed in Figure 5b. In Figure 5c we see that the remaining $^1H-^{31}P$ heteronuclear dipolar interactions are small under MAS as is evident from the lack of significant line narrowing under ^1H decoupling. The two ^{31}P peaks represent the HPO_4 (−2.4 ppm) and PO_4 (−0.9 ppm) tetrahedra. The isotropic chemical shift of the HPO_4 site is upfield from the PO_4 resonance and has approximately a 2:1 ratio, as expected from the X-ray crystal structure.

The primary difference between the two ^{31}P sites is their proximity to hydroxyl protons and interstitial water molecules. This is verified by the rate of the cross-polarization buildup from the ^1H to ^{31}P nuclei via the through-space dipolar coupling, which is inversely proportional to internuclear distance to the third power. The CP buildup study was performed on the centerband Hartmann−Hahn condition where $\omega_{1S} = \omega_{1I}$, in the rotating frame. The large $^{31}P-^{31}P$ distance allows us to assume that J transfer is negligible. The full series of CP spectra fits quite well to two Lorentzian components with varying intensities but constant chemical shifts and line widths. The extracted areas are plotted as a function of contact time (τ_{cp}) in Figure 6. The data were fit to the equation

$$M(\tau_{cp}) = M(1 - e^{-\tau_{cp}/T_{IS}})$$

which is valid in the high-spin−temperature limit while neglecting spin−lattice relaxation effects ($T_{1\rho}$) and effects due to differences in chemical shift between the phosphorus nuclei.[33,34] These fits give T_{IS} values of 470 and 626 μs for the

(33) Ding, S.; McDowell, C. A.; Ye, C. *J. Magn. Reson. Ser. A* **1994**, *109* (1), 6−13.
(34) Meier B. H. *Chem. Phys. Lett.* **1992**, *188* (3−4), 201−207.

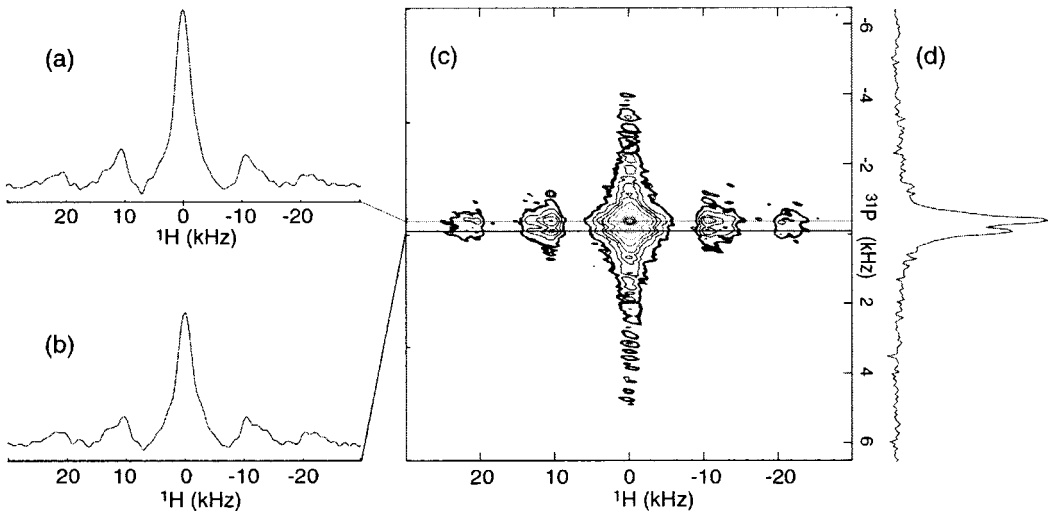

Figure 7. 2D WISE and extracted projections of $Ca_2In(PO_4)(HPO_4)_2 \cdot xH_2O$. ^1H "slices" taken at ^{31}P chemical shift values of (a) −2.4 ppm and (b) −0.9 ppm from the (c) 2D WISE spectrum. (d) Projection of the ^{31}P dimension.

HPO_4 and PO_4 ^{31}P nuclei, respectively. This observation confirms that the HPO_4 site is more strongly dipole coupled to protons than the PO_4 site.

A 2D WISE experiment allows the indirect detection of protons via their dipolar coupling to neighboring heteronuclear spins. In Figure 7, a $^1H-^{31}P$ 2D WISE spectrum is shown along with the associated 1D ^1H and ^{31}P projections. From the ^1H projections it is evident that both phosphate groups share a similar proton environment on NMR time scales. Both ^1H peaks in the WISE projection fit to a Lorentzian curve with roughly a 1.6 kHz line width. The similarity in proton environment and the projected ^1H line widths indicates that partial averaging from molecular motion and exchange occurs at rates comparable to NMR time scales ($^1H-^1H$ dipolar coupling for *static* interstitial water in a polycrystalline matrix is around 23.0 kHz[35]).

Conclusion

In contrast to most reported indium phosphates, which have three-dimensional frameworks, $Ca_2In(PO_4)(HPO_4)_2 \cdot H_2O$ is the first indium phosphate that is found to have an unusual pseudo layered framework. The layers are built from linear chains formed by corner-sharing (InO_6) octahedra and (PO_4)/(HPO_4) tetrahedra. A similar structure type has been found in the vanadium phosphate $Ca_2V(PO_4)(HPO_4)_2 \cdot H_2O$ and $Sr_2V(PO_4)_2(H_2PO_4)$.[15,16] The structures of some aluminum phosphates such as $Na_3Al(OH)(HPO_4)(PO_4)$[36] contain similar types of chains. However, (AlO_6) octahedra of neighboring chains directly link to each other by sharing corners.

Structural similarities have been reported among M(III) metal phosphates.[6,11,12,26] The preparation and characterization of mixed indium−iron phosphates $Ca_2(In_{1-x}Fe_x)(PO_4)(HPO_4)_2 \cdot H_2O$ ($x = 1, 0.5, 0$) confirm the structural similarities between In(III), V(III), and Fe(III) phosphates.

The two different phosphate moieties were confirmed by ^{31}P NMR; however, the 2D WISE experiment indicated no difference in proton environment. The line widths are consistent with some form of averaging; most likely it is a combination of chemical exchange and partial motional averaging of water and hydroxyl protons.

Acknowledgment. We are grateful to Dr. M. Watanabe and Dr. F. Kooli from NIRIM, Tsukuba, Japan, for their assistance in collecting the thermogravimetric data, and to Dr. Jones from the Department of Chemistry at Wake Forest University for the ICP analysis.

Supporting Information Available: Infrared absorption spectra, thermogravimetric and differential thermal analysis plots, temperature-dependent X-ray powder diffraction, and ICP elemental analyses. One X-ray crystallographic file containing data for the three compounds, in CIF format. This material is available free of charge via the Internet at http://pubs.acs.org.

IC9905906

(35) Duncan, T. M.; Dybowski, C. *Surf. Sci. Rep.* **1981**, *1*, 157.

(36) Lok, B. M.; Messina, C. A.; Patton, R. L.; Gajek, R. T.; Cannan, T. R.; Flanigen, E. M. *J. Am. Chem. Soc*. **1984**, *106* (20), 6092−6093.